

Article

Reliable Nanofabrication of Single-Crystal Diamond Photonic Nanostructures for Nanoscale Sensing

Mariusz Radtke ^{1,†}, Richard Nelz ¹, Abdallah Slablab ¹ and Elke Neu ^{1*}

¹ Saarland University, Faculty of Natural Sciences and Technology, Physics, Campus E2.6, 66123 Saarbrücken;

* Correspondence: elkeneu@physik.uni-saarland.de

† Current address: Department of Organic and Macromolecular Chemistry, Ghent University Krijgslaan 281, building S4, 9000 Gent, Belgium

Received: date; Accepted: date; Published: date

Abstract: In this manuscript, we outline a reliable procedure to manufacture photonic nanostructures from single-crystal diamond (SCD). Photonic nanostructures, in our case SCD nanopillars on thin ($< 1 \mu\text{m}$) platforms, are highly relevant for nanoscale sensing. The presented top-down procedure includes electron beam lithography (EBL) as well as reactive ion etching (RIE). Our method introduces a novel type of inter-layer, namely silicon, that significantly enhances the adhesion of hydrogen silsesquioxane (HSQ) electron beam resist to SCD and avoids sample charging during EBL. In contrast to previously used adhesion layers, our silicon layer can be removed using a highly-selective RIE step which is not damaging HSQ mask structures. We thus refine published nanofabrication processes to ease a higher process reliability especially in the light of the advancing commercialization of SCD sensor devices.

Keywords: top-down nanofabrication; single-crystal diamond; HSQ; Electron beam lithography; ICP RIE

1. Introduction

In recent decades, the use of optically active point defect, i.e. color centers, in single-crystal diamond (SCD) as atom-sized, solid-based quantum systems has emerged in various fields [1,2]. Applications span from quantum metrology (temperature [3], strain [4], electric [5] and magnetic fields [6]) to using color centers as spin qubits in quantum computing [7] and single photon sources for quantum communication [8,9]. The outstanding color center in diamond is the NV⁻ center due to its optically readable spin [10] and usage as sensor. For many of these applications, color centers will be incorporated into photonic nanostructures e.g. nanopillars [9] to ease fluorescence detection from the color centers and to enable e.g. scanning a color center close to a sample surface [6].

SCD's wide indirect bandgap of ~ 5.45 eV makes undoped SCD a good insulator [11]. Moreover, SCD shows a high chemical inertness. Both properties render fabricating SCD nanostructures challenging: Top-down methods for nanofabrication will use lithography, typically electron beam lithography (EBL), as well as etching. As the high chemical inertness of SCD prevents wet etching, only plasma etching, typically inductively coupled reactive ion etching (ICP-RIE), is applicable. Moreover, the insulating nature of SCD renders EBL highly challenging due to uncontrolled sample charging and the resulting deflection of the electron beam. A peculiarity of SCD nanofabrication arises also from the fact that only certain materials can efficiently serve as an etch mask in the high-bias, high-density plasmas necessary for anisotropic SCD etching [12]. The now state-of-the-art masks for SCD nanostructuring are EBL written structures consisting of hydrogen silsesquioxane (HSQ). HSQ is stable in anisotropic etch plasmas used for SCD etching; it etches an order of magnitude slower than SCD using typical etching recipes [12]. In general, HSQ enables to create very small mask structures down to 20 nm [13]. SCD structures etched using HSQ masks show smooth sidewalls [12]. Smooth sidewalls ensure low light scattering from photonic structures

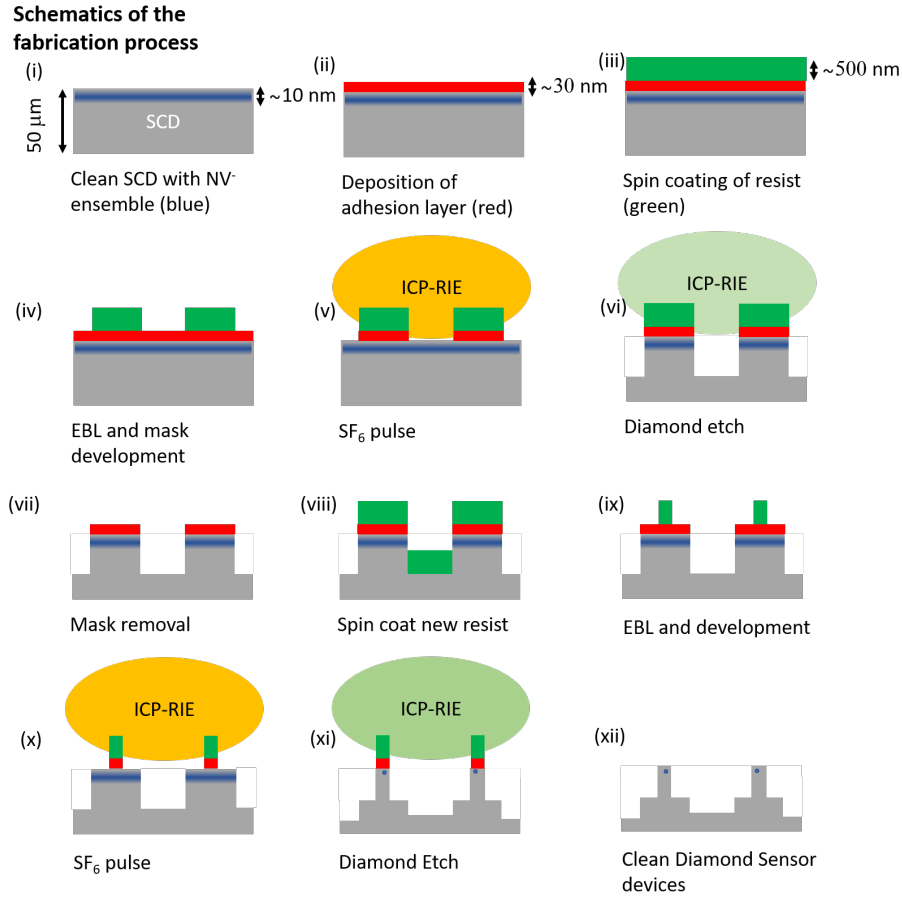


Figure 1. Step-wise description of our nanofabrication process to manufacture nanopillars on holding platforms as scanning probe sensors out of SCD. The layer in the schematics are not drawn to scale.

and defined waveguide properties. Consequently, HSQ masks enable etching almost cylindrical pillars with optimized shape and well-defined photonic properties [6,9,12,14,15]. On the other hand, we find that HSQ has a non-optimal adhesion to SCD. In previous work, this challenge has often been addressed using metallic inter-layers between HSQ and SCD e.g. titanium [16]. However, even very thin ($< 1 \text{ nm}$) metallic residuals on SCD surfaces strongly disturb color centers placed shallowly below the surface [17]. Consequently, any metallic residues are detrimental for the process and a metal-free process is highly desirable. Often, removing the metallic layer also requires wet chemical removal [16] or the use of toxic etch gases like chlorine [18]. The first can leave trace amounts of the etchant on the SCD surface and the second is technically demanding considering safety and reactor corrosion.

In this manuscript, we present a method to overcome two previously not satisfactorily addressed challenges in SCD nanofabrication namely sample charging as well as non-optimal resist adhesion. We use the optimized process to fabricate SCD scanning probes, namely nanopillars on thin holding platforms [6,16]. We thus reliably fabricate SCD nanostructures easing e.g. commercial fabrication of SCD scanning probes. Figure 1 depicts the steps of our nanofabrication process. We start with a clean SCD sample with a shallow NV⁻ layer (details on sample pre-treatment see Sec. 2) as mandatory for high resolution sensing. We use electron beam evaporation of silicon on SCD to form a de-charging and adhesive layer [Fig. 1 (ii), Sec. 3]. This layer will enable highly reliable spin coating of HSQ [Fig. 1 (iii)] as well as EBL [Fig. 1 (iv), Sec. 3]. Subsequently, we remove the silicon adhesion layer selectively using ICP-RIE without damage to the

HSQ mask [Fig. 1 (v)] and perform ICP-RIE of SCD to form the desired structures [Fig. 1 (vi), Sec. 4]. Our method eases manufacturing complex structures, like in our case nanopillars (diameter 200 nm) on top of SCD platforms (size of the platform $\sim 3 \times 20 \mu\text{m}$): In the first structuring step, we form the platforms [Fig. 1 (vi)]. The silicon adhesion layer survives the subsequent wet-chemical removal of the HSQ mask [Fig. 1 (vii)] and can be reused for a second round of processing [Fig. 1 (viii)-(xii)]. In this second processing, we form the pillars. We note when etching the platforms, the HSQ mask protects NV centers in the whole area of the micrometer-sized platform. During pillar etching, only NVs protected by the pillar mask survive the process and will be used as nanoscale sensors. The method presented here has been filed for a patent (EP19198772.6).

2. Sample pre-treatment

We purchase high-purity, (100)-oriented, chemical vapor deposited, SCD from Element Six (electronic grade quality, $[\text{N}]^s < 5 \text{ ppb}$, $\text{B} < 1 \text{ ppb}$). As we are aiming for free standing SCD devices consisting of nanopillars on platforms, the SCD plates (size $2 \times 4 \text{ mm}^2$) are polished down to thickness of $50 \mu\text{m}$ (Delaware Diamond Knives, US). The SCD surface shows an initial roughness of $R_a < 3 \text{ nm}$. As the mechanical polishing of the SCD can leave highly contaminated surfaces, we first wipe the sample surface using clean-room wipes and perform cleaning in an ultrasonic bath (solvents: isopropanol and acetone). We then clean the sample in boiling acids (1:1:1 mixture of sulfuric acid, perchloric acid and nitric acid, 5 ml each).

Mechanical polishing is suspected to introduce damage that potentially extends several micrometer deep into the SCD material [19,20]. In order remove this potentially damaged and strained material, we apply ICP-RIE to our SCD samples. We avoid the use of toxic or corrosive gases in the process following our previously published routine [21]. We use a Plasmalab 100 ICP-RIE reactor (Oxford instruments) and remove the topmost $3\text{--}5 \mu\text{m}$ of SCD from each side. We use a combination of $\text{SF}_6, \text{O}_2, \text{Ar}$ biased plasmas with mixed RF and ICP discharges. Following recent approaches [22,23], we terminate the etching using low-damage, 0 V bias plasma with pure oxygen. The use of such soft etching is motivated by the potential close-to-surface damage due to highly biased ICP etching [24]. We typically obtain very smooth surfaces with an rms roughness of $\sim 1 \text{ nm}$.

Using the above described procedure, we avoid creating NV centers in potentially damaged SCD. We form a homogeneous layer of NV^- centers by implanting nitrogen ions with a density of $2 \times 10^{11} \text{ ions/cm}^{-2}$ and an energy of 6 keV. During the implantation, the sample is tilted by 7° with respect to the ion beam to avoid ion channeling. The SCD sample is then annealed in vacuum at 800°C followed by an acid clean. This treatment will typically leave our sample with a mixed oxygen termination on the surface [25]. We find a contact angle for water of 67° [26] indicating a hydrophilic surface. As the electron beam resist we want to apply to the SCD is dissolved in methyl isobutyl ketone, a polar molecule, the resist's solvent has high affinity to hydrophilic surfaces. Despite the, in principle, fitting surface termination of the SCD sample we observe non-reliable adhesion when applying HSQ to the SCD surface.

3. Deposition of adhesion layer and HSQ mask structuring

Motivated by the lack of reliable adhesion of HSQ to clean SCD surfaces, we explore silicon as an inter-layer. We expect this layer to foster adhesion between polysilicate HSQ resist and the native oxide (SiO_2) on the layer. To deposit the silicon adhesion layer, we use electron beam evaporation at a pressure of 10^{-6} Torr and 10 kV acceleration voltage with elliptical beam scanning mode in an electron beam evaporator "Pfeiffer Classic 500 L" machine. For the present work, we choose a thickness of the silicon layer of 25 nm. We note that we also found sputtered silicon layers to efficiently foster adhesion between SCD and HSQ. However, the SCD surface was attacked during the sputtering process. This in our case led to

excess blinking and bleaching of NV^- centers in the final sensing devices and rules out this approach for our application. We also note that we tested spin coating Ti-prime as an adhesion promoter but did not obtain reliable results. We furthermore tested chromium layers as alternative to quickly oxidizing titanium layers [16]. Using this approach, we faced micromasking effects most probably arising from the incomplete, non-reliable wet-chemical removal of chromium layers. We note that our silicon layers still enable efficient HSQ adhesion weeks after deposition and storage under ambient conditions. We consequently conclude that the formation of a native oxide layer on the silicon, which will occur during storage at ambient conditions, is not detrimental. So, technically speaking evaporation of silicon layers can be performed in batch processes for several SCD samples which eases the fabrication workflow and reduces machine time. We note that adhesion of the silicon layer to SCD was very reliable and we never observed any hints of cracking or peeling throughout the whole process.

To manufacture etch masks based on HSQ, we use Fox 16 resist (Dow Corning) which we spin coat onto the SCD plate. To ease handling of our small SCD plates, we glue them to silicon carrier chips using crystalbond adhesive. Prior to spin coating, we heat the SCD sample on the silicon carrier for 10 minutes at 120°C to remove any moisture from the surface. We apply roughly 0.3 mL of Fox 16 solution to the SCD plate and spin-coat it at 1000 rpm for 10 seconds then increasing rotation speed to 3300 rpm for 60 s. Subsequently, we pre-bake the sample at 90°C for 5 minutes. We note that great care has been taken to not exceed the shelf life of the Fox 16 resist. As a result of the small size of our samples as well as the spin coating on already etched structures in the latter stages of our fabrication process, we can only estimate the thickness of the HSQ which shows a significant variation from sample to sample. From SEM images of pillar masks on platforms [see Fig. 2 (b)] we estimate a HSQ layer thickness of $\sim 0.9 \mu\text{m}$. Consequently, considering a pillar diameter of $\sim 200 \text{ nm}$, we demonstrate reliable adhesion of HSQ masks with an aspect ratio of 4.5.

We insert the SCD plate including the silicon carrier chip into our EBL machine (cold-cathode SEM, Hitachi S45000, equipped with RAITH Elphy software). We note that EBL of the spin coated HSQ layer has to be done directly after spin coating to avoid any reaction of HSQ with air. We perform EBL at 30 kV acceleration voltage and $20 \mu\text{A}$ extracting current. The working distance is kept at 15.3 mm for $400 \times 400 \mu\text{m}^2$ fields. During our device fabrication, larger structures, namely the rectangular holding platforms (size $\sim 3 \times 20 \mu\text{m}^2$) as well as masks for nanopillars (diameter 200 nm) were of interest. We write platforms using longitudinal writing mode and pillars using concentric writing modes. The doses for large structures were established to be optimal as $0.350 \mu\text{C}/\text{cm}^2$ and for pillar structures, with a variation with thickness of the HSQ layer, between 1.6 (planar SCD) and up to $5.0 \mu\text{C}/\text{cm}^2$ (pre-structured SCD with e.g. platforms).

We develop the HSQ in 25 % TMAH solution without swirling the solution. After 20 s the SCD sample is placed in ultra-pure 18 MOhm cm^{-1} MiliQ water and subsequently immersed several times in acetone and isopropanol. We note that the development has to take place directly after removing the SCD plate from the EBL vacuum chamber.

4. Selective ICP-RIE of adhesion layer and SCD structuring

A dedicated ICP/RIE plasma sequence based on O_2 -based etching of SCD, preceded by a short pulse of SF_6 plasma was designed. This sequence first selectively removes the silicon layer between the HSQ-based mask structures and subsequently enables highly anisotropic etching of SCD. The parameters of the plasmas are summarized in the Table 1. In the final process, we run the above mentioned sequence without removing the sample from the ICP-RIE reactor in-between the plasma steps to avoid any contamination.

Reliably removing the silicon layer without any residuals is vital to our process: The O_2 -based plasma, which we use for anisotropic SCD etching, does not etch silicon: We observe a partial etch stop as well as strong micromasking when applying the O_2 -based plasma without applying the SF_6 pulse [see Fig. 2

Table 1. Etching plasma parameters. SF₆ pulse used to selectively remove the evaporated silicon layer. The O₂ plasma is subsequently used as an anisotropic etch for SCD to form the platforms as well as the pillars.

Plasma	ICP Power W	RF Power W	Gas Flux sccm	Etch Rate nm/min	Pressure Pa
SF ₆ pulse	300	100	SF ₆ :25	Si: 1072 HSQ: 52	8.0
O ₂ plasma	500	200	O ₂ : 50	104	5.0

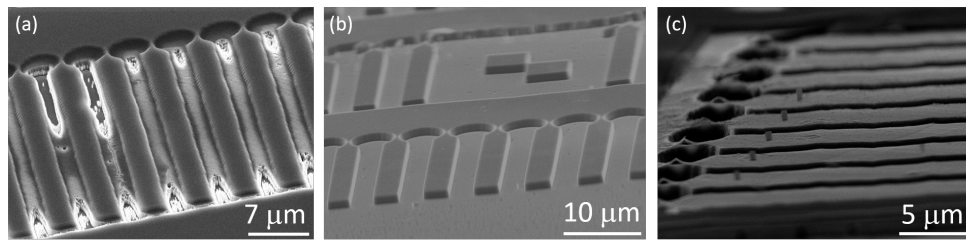


Figure 2. (a) Pattern of holding platforms etched with O₂ plasma without applying the SF₆ pulse plasma to remove the silicon layer. Strong micro-masking as well as a partial etch stop are visible (b) Devices at the intermediate stage of the process with etched-in platforms. Note that the SEM images shows the bare SCD structures. (c) HSQ masks for pillars etching written by EBL in this case on a freshly evaporated silicon layer.

(a)]. We deduce a complete and reliable removal of the silicon adhesion layer from two facts: First, in SEM images taken directly after the SF₆ pulse [see Fig. 3 (b)], a clear contrast between etched and non-etched areas is visible. Second, knowing that the O₂ plasma used to etch SCD is not etching the silicon layer, the absence of micromasking and very smooth surfaces in-between the etched structures [see Fig. 2 (b)] proves the complete removal of the silicon layer. We note that using pure SF₆ is vital to arrive at this result, as introduction of other gases (Argon, Oxygen) at this stage generated severe micromasking. Our SF₆ plasma removes the silicon layer while maintaining a 1:20 selectivity in favor of the HSQ mask. For our process this means that during removal of the 25 nm thick silicon adhesion layer less than 2 nm of the HSQ mask, which in our case is several hundreds of nanometer thick, will be lost. This result corresponds well to similar plasmas obtained in different systems showing highly selective silicon etching while conserving SiO₂ (in our case HSQ) [27]. Using EDX, we check that there is no silicon contamination on the etched SCD after the O₂-based plasma (see Fig. 4). We investigate the SF₆-based etching process by means of optical emission spectroscopy shown in Fig. 3 (a). In the spectrum a series of emission lines corresponding to fluoride (F⁻) were observed [28]. We attribute the etching of silicon to this F⁻ ions. We furthermore observe no or minor etching of SCD during the SF₆ pulse and no roughening of the exposed SCD surface.

After successfully structuring our SCD platforms, we remove HSQ residuals using HF-based buffered oxide etch by immersion of SCD for 20 minutes in the solution. Though this step removes the native oxide from our silicon adhesion layer, the layer itself survives the process as clearly discernible from the EDX imaging in Fig. 4 (b). Consequently, it can be re-used for consecutive steps. We now spin-coat HSQ again, which in our case forms a layer on top as well as in-between the platforms. We then re-employ EBL to create pillar masks on the platforms [see Fig. 2 (c)]. We repeat the etching to transfer the pillar mask into the SCD platform creating almost cylindrical pillars.

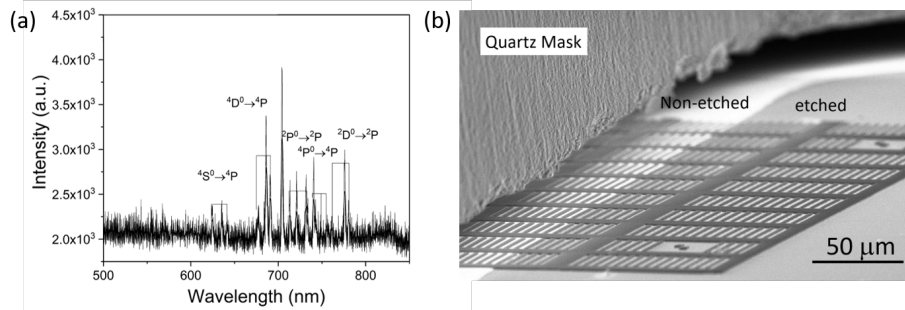


Figure 3. (a) Optical emission spectrum of the SF_6 pulse plasma step indicating presence of fluoride (F^-) species responsible for selective removal of silicon from the SCD surface. (b) Scanning electron microscope (SEM) image of SCD surface with HSQ structures, here platforms, after SF_6 pulse. A part of the platforms is covered with a quartz plate (marked in the image) during the SF_6 pulse. The strongly reduced brightness of the etched surface in contrast to non-etched surface indicates the complete removal of the silicon adhesion layer. We furthermore observe no or minor etching of SCD during the SF_6 pulse and no roughening of the exposed SCD surface.

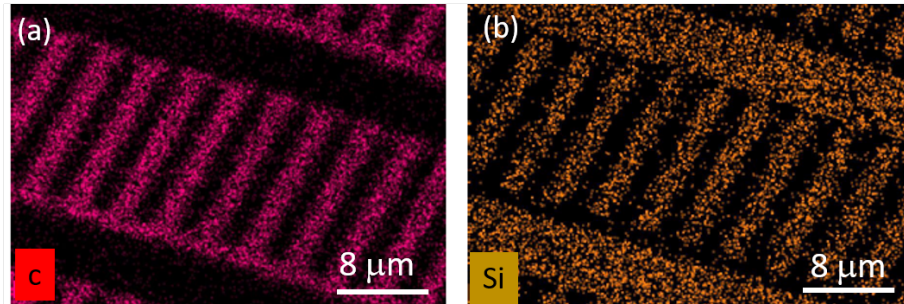


Figure 4. Energy dispersive X-ray fluorescence mapping of SCD cantilevers prepared by the presented method. The EDX mapping has been performed after the SF_6 plasma, the O_2 plasma etching the SCD structures (parameters see Tab. 1) and the wet chemical removal of residual HSQ. (a) carbon signal, (b) silicon signal. The two maps show complementary images, clearly indicating that in-between the platforms, we find bare SCD (carbon) with no silicon signal while on the platform, the silicon adhesion layer survived and is ready to be used in the next processing step.

5. Final devices and device characterization

To obtain clean SCD devices, we remove all HSQ residuals using HF-based buffered oxide etch. We immerse the SCD into buffered oxide etch for 20 min which removes the HSQ as well as any native oxide on the silicon layer. Afterwards, we immerse the SCD sample in 3M potassium hydroxide at 80°C for 30 minutes to remove the silicon adhesion layer and reveal the clean SCD structures. After this process, we repeat the 3-acid cleaning described above before characterizing the photoluminescence (PL) of NV⁻ centers in the SCD nanostructures. Figure 5 (a) display devices obtained using this process. We note that to obtain free standing devices which we mount to quartz capillaries as holders [see Fig. 5 (b)] the SCD plate has to be thinned from the non-structured side until the devices are fully released. For more details on the mounting see Ref. [16]. To this end, we employ previously published deep-etching routines [21] which are beyond the scope of this manuscript.

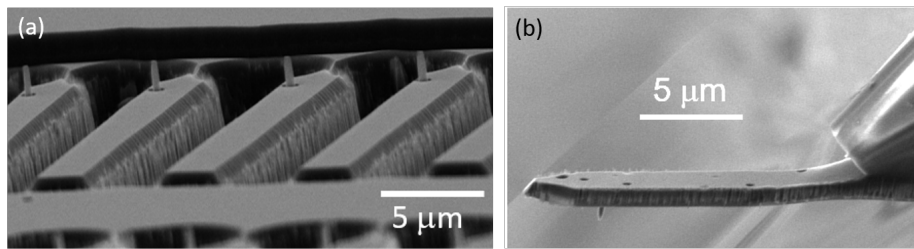


Figure 5. Scanning probe devices manufactured using the described nanofabrication process. (a) pillars on platforms. The shown devices still need thinning of the SCD plate from the backside to release the devices. (b) mounted SCD scanning probe. On the right hand side, a quartz capillary is visible that serves as a holder to mount the device to a scanning probe microscope.

To investigate the photonic properties of our SCD nanostructures, we use a custom-built confocal microscope (numerical aperture 0.8). Details of the setup are given in Refs. [22,29–31].

We first measure confocal PL maps of the structures [see Fig. 6 (a) and (b)] excited at 532 nm with a power of 500 μ W. We clearly observe intense PL (\sim 100 kcps) originating from single NV⁻ centers in the pillars [see Fig. 6 (a)]. We estimate the maximum achievable PL of the NV⁻ centers to be >300 kcps comparable to previous work [16]. In addition, we investigate the background PL from the etched surface (\sim 1 kcps) which is negligible compared to the NV⁻ center PL from the pillar [see Fig. 6 (b)]. Keeping background PL from etched surfaces low is important as it limits the signal-to-background ratio and consequently the achievable magnetic field sensitivity [32]. Fig. 6 (c) shows an exemplary optically detected magnetic resonance (ODMR) measured on single NV⁻ centers in the structures. Here we measure an ODMR contrast of \sim 15%. By investigating the coherence of the NV⁻ centers in the nanostructures, we find a coherence time of $T_2 \leq 10 \mu$ s. We attribute this to the NV⁻ centers' proximity to the surface which is in a good agreement with results from other groups measuring the coherence of shallow NV⁻ centers in 3-acid cleaned SCD [33]. Considering the already low T_2 , we cannot fully exclude a negative influence of the structuring on T_2 .

6. Summary and conclusion

In this study, we present a reliable technology for nanofabrication of SCD structures. We use our method to manufacture SCD scanning probes with shallowly embedded negative nitrogen vacancies. The method introduces an evaporated silicon adhesion layer on the SCD surface to ease adhesion and EBL with spin-coated HSQ-based Fox 16 resist. We present a methodology for the selective removal of our silicon adhesive/decharging layer with SF₆ plasma. In areas protected by the HSQ mask, silicon layer survives etching as well as wet chemical removal of the residual HSQ mask and can be re-used for

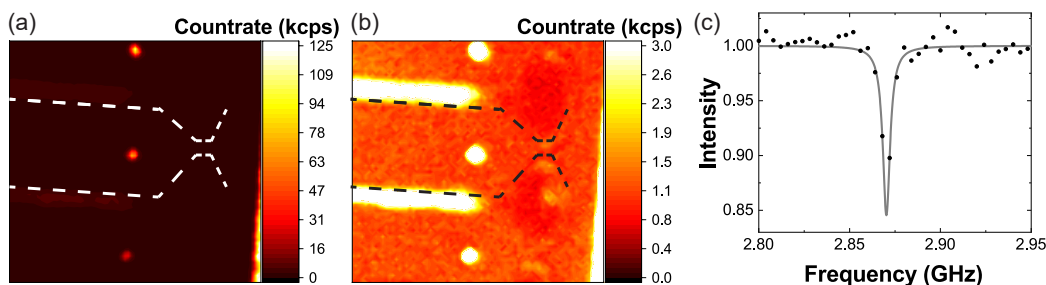


Figure 6. (a)+(b) PL map of SCD platforms with individual nanopillars fabricated with the process described in Sec. 4. The outer edge of the holding platform is indicated using a dashed line, while the pillars appear as bright spots. To enable comparing the background PL from the platforms with the PL of a few NV[−] centers in the pillars, we show the same PL map with two different scaling: individual NV[−] centers in the pillars show PL countrates above 125 kcps at an excitation power of 500 μ W at 532 nm [part (a)]. In Contrast, in part (b) it is clearly discernible that the cantilevers show only a weak PL of \sim 1 kcps. The enhanced background in-between the platform arises from a slight roughening between the structures. We detect NV[−] PL in the wavelength range $>$ 650 nm. (c) shows an exemplary optically detected magnetic resonance (ODMR) of one of the NV[−] centers in the pillar. The resonance (without an external magnetic field) at 2.87 GHz is clearly visible and has a contrast of \sim 15%.

further nanofabrication, in our case for pillars on SCD platform. The shallowly implanted NV[−] centers survived the nanofabrication process. We have found this method to be reliable, which is a considerable advancement in SCD nanofabrication technology that can be expanded to various kinds of SCD structures including SCD cantilever or cavity structures (e.g. photonic crystals).

Acknowledgements

We would like to acknowledge Dr. Ing. Sandra Wolff (TU Kaiserslautern, Germany) for help with electron beam evaporation, Jörg Schmauch (INM, Germany) for his help with acquiring high-quality SEM images and Dr. Rene Hensel (INM, Germany) for granting access to the ICP/RIE reactor. We acknowledge Michel Challier for his assistance and Dr. Andreas Ruh (Saarland University, Germany) for his help with EDX. We gratefully acknowledge cooperation and fruitful discussion with QNAMI (Basel) especially with Dr. Felipe Favaro De Oliveira and Prof. Dr. Patrick Maletinsky on the evaluation of our novel nanofab method. We acknowledge funding via a NanoMatFutur grant of the German Ministry of Education and Research (FKZ13N13547). We note that the results presented in this study are filed for a patent, application number: EP19198772.6.

7. References

1. Atatüre, M.; Englund, D.; Vamivakas, N.; Lee, S.Y.; Wrachtrup, J. Material platforms for spin-based photonic quantum technologies. *Nature Reviews Materials* **2018**, *3*, 38. doi:10.1038/s41578-018-0008-9.
2. Casola, F.; van der Sar, T.; Yacoby, A. Probing condensed matter physics with magnetometry based on nitrogen-vacancy centres in diamond. *Nature Reviews Materials* **2018**, *3*, 17088.
3. Kucsko, G.; Maurer, P.; Yao, N.; Kubo, M.; Noh, H.; Lo, P.; Park, H.; Lukin, M. Nanometre-scale thermometry in a living cell. *Nature* **2013**, *500*, 54–58. doi:10.1038/nature12373.
4. Teissier, J.; Barfuss, A.; Appel, P.; Neu, E.; Maletinsky, P. Strain Coupling of a Nitrogen-Vacancy Center Spin to a Diamond Mechanical Oscillator. *Phys. Rev. Lett.* **2014**, *113*, 020503. doi:10.1103/PhysRevLett.113.020503.

5. Dolde, F.; Doherty, M.W.; Michl, J.; Jakobi, I.; Naydenov, B.; Pezzagna, S.; Meijer, J.; Neumann, P.; Jelezko, F.; Manson, N.B.; Wrachtrup, J. Nanoscale Detection of a Single Fundamental Charge in Ambient Conditions Using the NV- Center in Diamond. *Phys. Rev. Lett.* **2014**, *112*, 097603. doi:10.1103/PhysRevLett.112.097603.
6. Maletinsky, P.; Hong, S.; Grinolds, M.; Hausmann, B.; Lukin, M.; Walsworth, R.; Loncar, M.; Yacoby, A. A robust scanning diamond sensor for nanoscale imaging with single nitrogen-vacancy centres. *Nat. Nanotechnol.* **2012**, *7*, 320–324. doi:10.1038/NNANO.2012.50.
7. Neumann, P.; Kolesov, R.; Naydenov, B.; Beck, J.; Rempp, F.; Steiner, M.; Jacques, V.; Balasubramanian, G.; Markham, M.L.; Twitchen, D.J.; Pezzagna, S.; Meijer, J.; Twamley, J.; Jelezko, F.; Wrachtrup, J. Quantum register based on coupled electron spins in a room-temperature solid. *Nat. Phys.* **2010**, *6*, 249–253. doi:[10.1038/NPHYS1536].
8. Kurtsiefer, C.; Mayer, S.; Zarda, P.; Weinfurter, H. Stable Solid-State Source of Single Photons. *Phys. Rev. Lett.* **2000**, *85*, 290–293. doi:10.1103/PhysRevLett.85.290.
9. Babinec, T.; Hausmann, B.; Khan, M.; Zhang, Y.; Maze, J.; Hemmer, P.; Loncar, M. A diamond nanowire single-photon source. *Nature Nanotech.* **2010**, *5*, 195–199. doi:10.1038/NNANO.2010.6.
10. Gruber, A.; Dräbenstedt, A.; Tietz, C.; Fleury, L.; Wrachtrup, J.; von Borczyskowski, C. Scanning confocal optical microscopy and magnetic resonance on single defect centers. *Science* **1997**, *276*, 2012–2014. doi:DOI: 10.1126/science.276.5321.2012.
11. Zaitsev, A. *Optical Properties of Diamond: A Data Handbook*; Springer, 2001.
12. Hausmann, B.J.; Khan, M.; Zhang, Y.; Babinec, T.M.; Martinick, K.; McCutcheon, M.; Hemmer, P.R.; Loncar, M. Fabrication of diamond nanowires for quantum information processing applications. *Diamond Relat. Mater.* **2010**, *19*, 621 – 629. doi:10.1016/j.diamond.2010.01.011.
13. Grigorescu, A.; Hagen, C. Resists for sub-20-nm electron beam lithography with a focus on HSQ: state of the art. *Nanotechnology* **2009**, *20*, 292001.
14. Neu, E.; Appel, P.; Ganzhorn, M.; Miguel-Sanchez, J.; Lesik, M.; Mille, V.; Jacques, V.; Tallaire, A.; Achard, J.; Maletinsky, P. Photonic nano-structures on (111)-oriented diamond. *Appl. Phys. Lett.* **2014**, *104*, 153108. doi:<http://dx.doi.org/10.1063/1.4871580>.
15. Fuchs, P.; Challier, M.; Neu, E. Optimized single-crystal diamond scanning probes for high sensitivity magnetometry. *New Journal of Physics* **2018**, *20*, 125001. doi:10.1088/1367-2630/aaf0c5.
16. Appel, P.; Neu, E.; Ganzhorn, M.; Barfuss, A.; Batzer, M.; Gratz, M.; Tschöpe, A.; Maletinsky, P. Fabrication of all diamond scanning probes for nanoscale magnetometry. *Review of Scientific Instruments* **2016**, *87*, 063703. doi:<http://dx.doi.org/10.1063/1.4952953>.
17. Lillie, S.E.; Broadway, D.A.; Dontschuk, N.; Zavabeti, A.; Simpson, D.A.; Teraji, T.; Daeneke, T.; Hollenberg, L.C.; Tetienne, J.P. Magnetic noise from ultrathin abrasively deposited materials on diamond. *Physical Review Materials* **2018**, *2*, 116002.
18. Xie, L.; Zhou, T.X.; Stöhr, R.J.; Yacoby, A. Crystallographic orientation dependent reactive ion etching in single crystal diamond. *Advanced Materials* **2018**, *30*, 1705501.
19. Volpe, P.N.; Muret, P.; Omnes, F.; Achard, J.; Silva, F.; Brinza, O.; Gicquel, A. Defect analysis and excitons diffusion in undoped homoepitaxial diamond films after polishing and oxygen plasma etching. *Diamond Relat. Mater.* **2009**, *18*, 1205 – 1210. doi:<http://dx.doi.org/10.1016/j.diamond.2009.04.008>.
20. Naamoun, M.; Tallaire, A.; Silva, F.; Achard, J.; Doppelt, P.; Gicquel, A. Etch-pit formation mechanism induced on HPHT and CVD diamond single crystals by H₂/O₂ plasma etching treatment. *physica status solidi (a)* **2012**, *209*, 1715–1720. doi:10.1002/pssa.201200069.
21. Challier, M.; Sonusen, S.; Barfuss, A.; Rohner, D.; Riedel, D.; Koelbl, J.; Ganzhorn, M.; Appel, P.; Maletinsky, P.; Neu, E. Advanced Fabrication of Single-Crystal Diamond Membranes for Quantum Technologies. *Micromachines* **2018**, *9*, 148. doi:10.3390/mi9040148.
22. Radtke, M.; Nelz, R.; Render, L.; Neu, E. Plasma surface treatments and photonic nanostructures for shallow nitrogen vacancy centers in diamond. *manuscript in preparation* **2019**.

23. de Oliveira, F.F.; Momenzadeh, S.A.; Wang, Y.; Konuma, M.; Markham, M.; Edmonds, A.M.; Denisenko, A.; Wrachtrup, J. Effect of low-damage inductively coupled plasma on shallow nitrogen-vacancy centers in diamond. *APPLIED PHYSICS LETTERS* **2015**, *107*, 073107. doi:{10.1063/1.4929356}.

24. Kato, Y.; Kawashima, H.; Makino, T.; Ogura, M.; Traoré, A.; Ozawa, N.; Yamasaki, S. Estimation of Inductively Coupled Plasma Etching Damage of Boron-Doped Diamond Using X-Ray Photoelectron Spectroscopy. *physica status solidi (a)* **2017**, *214*, 1700233.

25. Krueger, A.; Lang, D. Functionality is Key: Recent Progress in the Surface Modification of Nanodiamond. *ADVANCED FUNCTIONAL MATERIALS* **2012**, *22*, 890–906.

26. Challier, M.; Nelz, R.; Kiendl, B.; Slablab, A.; Radtke, M.; Mueller, F.; Krueger, A.; Neu, E. Wet chemical fluorine treatment of diamond: towards hydrophobic diamond nano-devices for single NV sensing. *manuscript in preparation* **2019**.

27. Morshed, M.; Daniels, S. Electron Density and Optical Emission Measurements of SF₆ /O₂ Plasmas for Silicon Etch Processes. *Plasma Science and Technology* **2012**, *14*, 316–320. doi:10.1088/1009-0630/14/4/09.

28. dAgostino, R.; Flamm, D.L. Plasma etching of Si and SiO₂ in SF₆ mixtures. *Journal of Applied Physics* **1981**, *52*, 162–167. doi:10.1063/1.328468.

29. Nelz, R.; Fuchs, P.; Opaluch, O.; Sonusen, S.; Savenko, N.; Podgursky, V.; Neu, E. Color center fluorescence and spin manipulation in single crystal, pyramidal diamond tips. *Applied Physics Letters* **2016**, *109*, 193105. doi:<http://dx.doi.org/10.1063/1.4967189>.

30. Nelz, R.; Görlitz, J.; Herrmann, D.; Slablab, A.; Challier, M.; Radtke, M.; Fischer, M.; Gsell, S.; Schreck, M.; Becher, C.; others. Toward wafer-scale diamond nano-and quantum technologies. *APL Materials* **2019**, *7*, 011108.

31. Nelz, R.; Radtke, M.; Slablab, A.; Kianinia, M.; Li, C.; Xu, Z.Q.; Bradac, C.; Aharonovich, I.; Neu, E. Near-field energy transfer between a luminescent 2D material and color centers in diamond. *arXiv preprint arXiv:1907.12248* **2019**.

32. Rondin, L.; Tetienne, J.P.; Hingant, T.; Roch, J.F.; Maletinsky, P.; Jacques, V. Magnetometry with nitrogen-vacancy defects in diamond. *Rep. Prog. Phys.* **2014**, *77*, 056503.

33. Sangtawesin, S.; Dwyer, B.L.; Srinivasan, S.; Allred, J.J.; Rodgers, L.V.; De Greve, K.; Stacey, A.; Dontschuk, N.; O'Donnell, K.M.; Hu, D.; others. Origins of diamond surface noise probed by correlating single spin measurements with surface spectroscopy. *arXiv preprint arXiv:1811.00144* **2018**.